Cheiron School 2015

BL10XU: High Pressure Research

Outline

The undulator beamline BL10XU is dedicated for x-ray diffraction experiments at high pressure and low/high temperature using diamond anvil cells (DAC) (Figure 1) [Ohishi *et al.* (2008) *High Press. Res.*, **28**, 163.]. Monochromatic x-ray diffraction using synchrotron radiation plays an essential role in structural determination of crystalline materials. High pressure is possible to change physical, chemical, and structural characteristics of materials through a change of the distance between atoms (or molecules). The high-pressure properties are drastically different from those known at ambient pressure. Pressure serves as a versatile tool in material research, and it is also important in the investigation of the deep interior of the Earth and planets. To learn high-pressure phenomena in the BL practice course, in-situ high-pressure x-ray diffraction experiments will be performed using a combination of synchrotron radiation and a DAC technique.

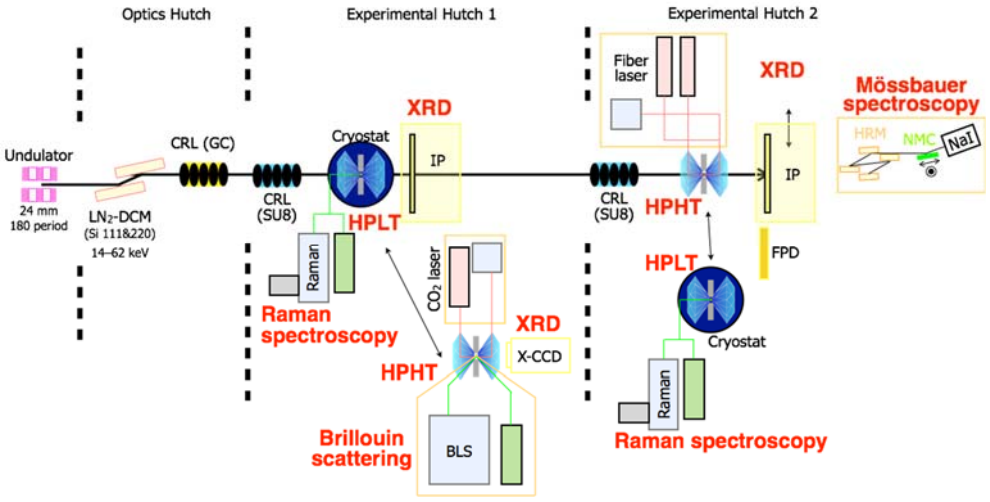

Figure1. Schematic layout of beamline BL10XU.

Diamond anvil cell

Diamond anvil cell is one of high-pressure generation techniques by static compression. The sample is placed in a pressure chamber created between the flat parallel faces (culets) of two opposed diamond anvils and the hole penetrating a hardened metal foil (the gasket) (Figure 2). Pressure is applied by forcing the diamonds together. Diamond is the premier anvil material because of hardest substance and transparency to electromagnetic radiation over a wide spectral range from the infrared to hard X-rays.

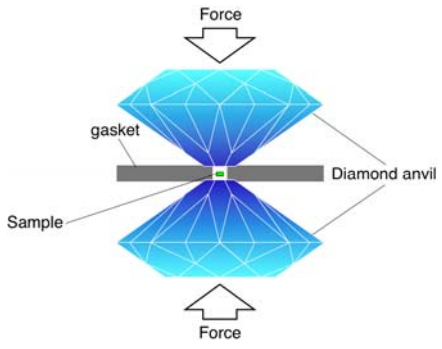

Figure 2. Diamond-anvil cell

Energy calibration

Precise x-rays energy is essential to determine lattice parameters or crystal structures of materials in monochromatic x-ray diffraction measurement. The x-rays energy/wavelength can be obtained using a diffraction standard material with well-established lattice parameter, such as cerium oxide (celia, CeO_2), as the x-ray wavelength is linked to crystal lattice spacing by Bragg's law. In this practice, the energy of the incident monochromatic x-ray beam is tuned to 30 keV (0.4133 Å). Also, the precise sample-to-detector distance is required in monochromatic x-ray diffraction measurement because of eliminating the uncertainty of the distance for the error in the *d*-spacing.

For calibration, two-film cassette method is used by recording a diffraction pattern on a flat detector and giving a second pattern after the detector moves parallel to the incident x-ray beam by an accurately known distance ΔL. The diffraction angle θ is then given by the relation

$$\tan 2\theta = \frac{R_1}{L} = \frac{R_2 - R_1}{\Delta L}$$

$$L = \frac{R1}{R2 - R1}\Delta L$$

, where R_1 and R_2 are the diffraction ring radius for the sample-to-camera distances L and $L + \Delta L$, respectively.

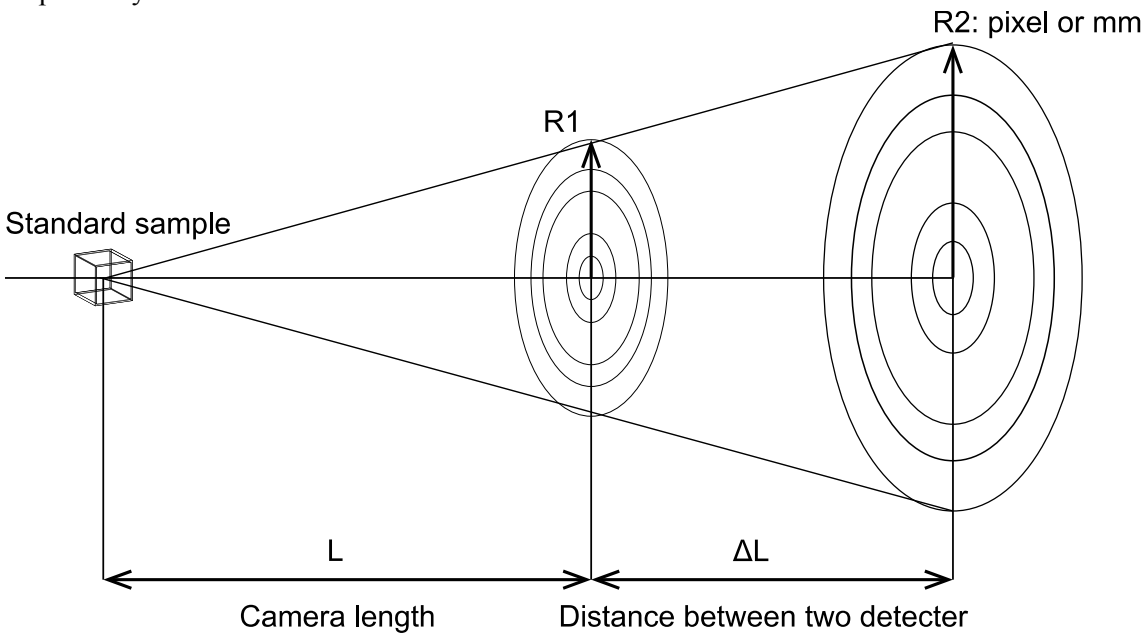

Figure3. Schematic image of camera length calibration.

– Practice –

1. Observe a crystallization of liquid Argon, and confirm the solid phase structure at high pressure with using DAC.
2. Obtain the parameters of Equation of State (EOS) for solid dense Argon from in-situ X-ray diffraction data.

1) Why Argon?

General introduction

Here, we focus on the high pressure behavior of dense Argon (Ar). There are a lot of experimental and theoretical studies to investigate the liquid and solid Ar density and thermal properties at high pressure with following reasons. (1) Ar is the rare-gas, and the abundance of Ar is the 3th-highest in the dry air. We can get Ar at a reasonable price, (2) its chemically inert behavior, (3) its molecular simplicity, such as monoatomic, nonpolar, and closed-shell electronic configuration. Therefore, Ar is commonly used as a reference material to calibrate and check the consistency of the new measurement system or calculation method.

Phase relations of Ar at high pressure

The melting curve of Ar was determined up to 80 GPa with DAC [Boehler *et al.* (2001) *Phys. Rev. Lett.,* **86**, 5731.]. The phase relation of Ar was shown in Figure 3. In previous experimental study, no structural transition was observed, and fcc Ar is stable over Mbar pressure condition at low to high temperature. McMahan (1986) [*Phys. Rev. B.,* **33**, 8.] predicted the structural transition and metallization at high pressure at 0 K with first principle calculation. He indicated that fcc to hcp transition is occurred at 230 GPa. Ar would be metallized in the hcp stable range. Hcp phase is stable up to 970 GPa, and undergoes a phase transition to bcc. Finally at 2200 GPa, high pressure fcc phase would be observed. Today, we try to check the pressure of liquid to solid transition. Finger et al. (1981) [*Appl. Phys. Lett.*, **39**, 892.] and Datchi et al. (2000) [*Phys. Rev. B.* **61**, 6535.] revealed the transition pressure is 1.15-1.3 GPa. Is it true in your experiment?

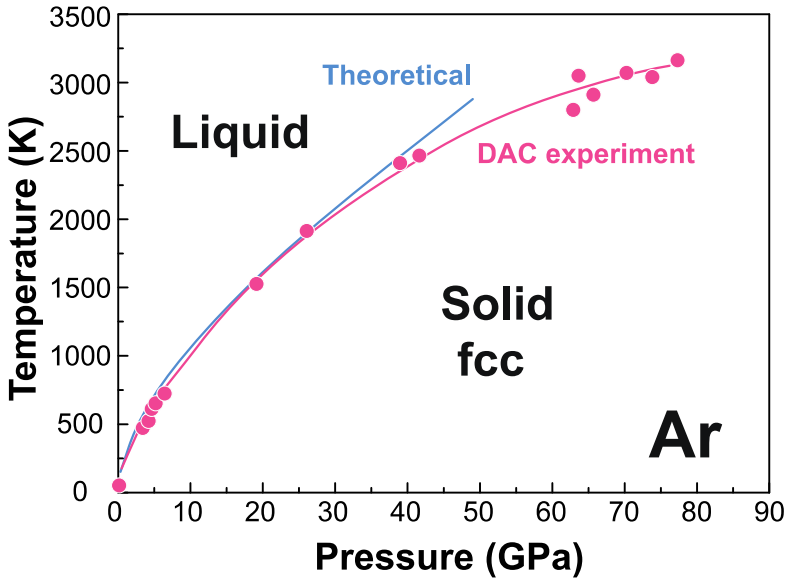

Figure 4. Melting curve of Ar at high pressure [*Boehler et al.* (2001) *Phys. Rev. Lett., **86**, 5731.*]

Implication for the Earth's interior~Missing Ar problem

Allegre et al. (1996) [*Geo. Res. Lett.,* **12**, 24, 3555.] suggested that almost half of ^{40}Ar in the whole Earth are missing, and these missing ^{40}Ar would be hidden in the Earth's lower mantle. ^{40}Ar in the present Earth was produced by radioactive delay of ^{40}K. We can calculate the amount of Ar as 1.16 times of present K. K content in the bulk Earth was assumed as 1.16 times of present ^{40}K. The present K content could be estimated from K/U ration (12700) by weight from primitive mantle composition predicted from Mid-ocean ridge basalt and ocean-island basalt. Sold Earth have 20-22.5 ppm U from meteorite composition, therefore, K abundance can be judged to be 250-285 ppm in the bulk Earth. From this consideration, ^{40}Ar has been produced 140-150×10^{18} g. ^{40}Ar are 66×10^{18} g in the air, and about 9-12×10^{18} g and 7.3-9.3×10^{18} g in each continental crust and upper mantle (Figure 5). Therefore, 60-80×10^{18} g are hidden by the reservoir in the deep Earth's interior, lower mantle or metallic core. Ar is well known that liquid iron (Earth's core) rarely react with Ar.

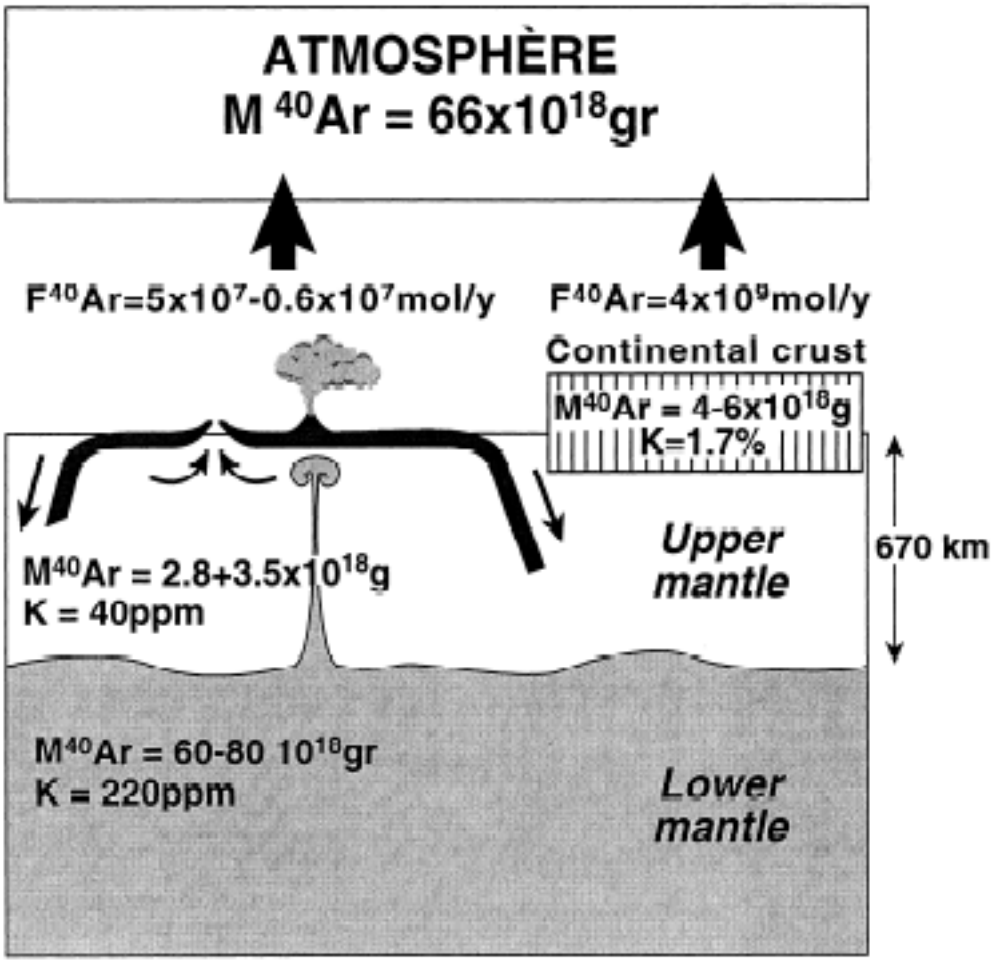

Figure 5. Hidden Ar in the lower mantle [*Allegre et al.* (1996) *Geo. Res. Lett.,* ***12****, 24, 3555*.]

Jephcoat (1998) [*Nature.* **393,** 355.] suggested that solid pure Ar in the Earth's lower mantle from their determined melting curve of noble gases and compressibility. They found solid-liquid transition is occurred at around 25 GPa (720 km depth, lower mantle) on the Geotherm. Their scenario is that Ar has been produced from K in both lower mantle and the core. Ar is solidified at lower mantle and liquid outer core. Ar is enough denser than the surrounding mantle to sink to the bottom of the mantle (Figre 6). On the other hands, solid Ar float from surrounding liquid core to top of the core. Ar will have been "confined" at the core mantle boundary over 4 billion years.

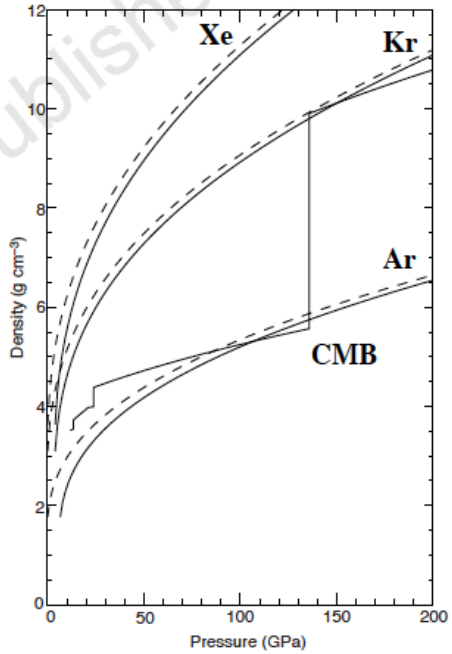

Figure 6. Hidden Ar in the lower mantle [*Jephcoat (1998)* [*Nature.* ***393****, 355.*]

2) Sample preparation

In general experiments with DAC technique, samples are set up in a chamber created between the culets of two opposed diamond anvils and the gasket hole. The gasket in anvil devices serves three critical functions: (1) encapsulating the sample, (2) building a gradient from ambient to the peak pressure, and (3) supporting the tip of anvils. Gasket material, hole size of sample chamber, and thickness are critical for generating high pressure.

What about is the gasket condition in this practice? Let's ask to the staff!!:
Material:
Initial gasket thickness:
Initial gasket hole size:

The pressure limit is depend on the culet size of diamond anvil as following;

$$\text{Pressure} = \frac{\text{Force}}{\text{Area}}.$$

Pressure limitation vs. culet size relations are shown in Table 1.

Table 1.

Culet size	Pressure limitation
600 μm	< 20 GPa
450 μm	40-50 GPa
300 μm	70-80 GPa
150 μm	~140 GPa
Smaller	>300 GPa !

Today, high pressure condition is generated with a gas-membrane DAC. Ar gas was loaded in a chamber hole drilled in a Re foil using a high-pressure gas-loading technique at 200 MPa, together with tiny ruby chips for a pressure marker. Generally, we load samples together with some soft pressure medium to distribute hydrostatic pressure condition, such as NaCl, KCl, gas, gel, or ethanol-methanol mixture.
However, in this case, we operate our high pressure experiment without pressure medium, because Ar itself is a good soft pressure medium.

3) XRD data collection at ambient and high pressures

In-situ high-pressure XRD measurements are carried out with the following steps:
(1) At first, take XRD pattern at current pressure,
(2) Compress DAC to the interest pressure carefully, and determine pressure with ruby scale,
(3) Collect of XRD images with the imaging plate detector at each pressure with increasing pressure.
(4) Check the pressure of liquid-solid pressure transition, and confirm the structure of solid Ar.
(5) Obtain XRD images at pressure intervals up to about 40 GPa.

4) High-pressure generation and pressure measurement

In a gas-membrane DAC, pressure is generated online, smoothly, and remotely through controlling the gas pressure in a membrane.

Pressure in the DAC is determined by ruby pressure scale [Mao *et al.* (1978) *J. Appl. Phys*. **49**, 3276.]. The ruby scale, which has been calibrated against primary shock-wave experiments on several metals, is commonly used for DACs: the pressure-shift of ruby fluorescence wavelength can be easily probed with a laser beam through the diamond window. Determine the pressure with empirical quasi-linear relationship: P (GPa) = $1904[(\lambda/\lambda_0)^B - 1] / B$, where $B = 5$ for non-hydrostatic conditions, for the correlation of the measured wavelength shift λ (in nm) of the R_1 line with applied pressure.

5) Data analysis and peak indexing

The basic principle of the X-ray diffraction is the Bragg's law: $\lambda = 2d\sin\theta$, where λ is the wavelength of the X-ray, d the lattice spacing, θ the angle of the incident beam and the diffracting lattice plane. The diffraction peaks are observed when the d-spacing satisfied the Bragg's law.

First, convert the X-ray image to conventional one-dimensional X-ray pattern with the software. Next, calculate d-spacing for each peak from 2θ value using the Bragg's law. Then,

perform peak indexing. Finally, refine the unit-cell parameter and volume.

Note that Ar has face-centered cubic (fcc) structure with space group of *Fm*3*m*. From equation of state, the lattice parameter of Ar is 5.3166 Å at ambient condition [Jephcoat (1998) *Nature*. **393**, 355.].

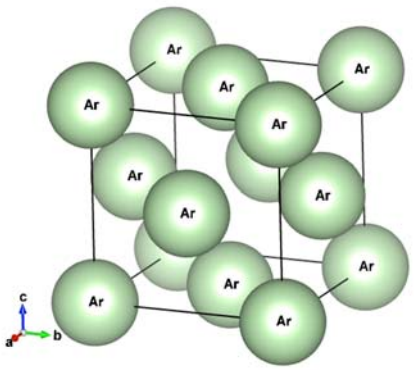

Figure 5. Crystal structure of sold fcc Ar.

5) Determination of the EOS parameters

An EOS is the relationships among the thermodynamic parameters volume, pressure, or temperature. The EOS is useful to describe the properties of solid, fluid, and even the interior of planets and stars. In this practice, obtain the EOS parameters of zero-pressure bulk modulus and its pressure derivative for a sold Ar phase from pressure-volume data at room temperature. Plot the *P*-*V* data, and then fit the EOS with the Birch-Murnaghan equation.

Note that the Birch-Murnaghan equation of state is based on the Eulerian strain [Birch (1952) *J. Geophys. Res*. **57**, 227.] and is widely used for mineralogists:

$$P = 3K_{T0}/2\ [(V_0/V)^{7/3} - (V_0/V)^{7/3}]\{1 - 3/4(4 - K'_{T0})[\ (V_0/V)^{2/3} - 1]\}$$

, where P is pressure, K_T zero-pressure bulk modulus, K'_T its pressure derivative, V the volume at P, and the subscript "0" refers to ambient pressure conditions.

6) Comparison with other materials

Compare the EOS parameters of Ar with other materials and rare-gas solids. The parameters for ionic, covalent, and metal crystals are given in table.

Table 2

Material	K_0 (GPa)	K'_0	Ref.
Diamond	444.5	3.98	[1]
Na	6.31	3.886	[2]
Si	97.9	4.16	[3]
Al	73	4.54	[4]
Au	167	5.46	[5]
Pt	277	5.08	[4]

MgO	160.2	3.99	[6]
Al_2O_3	253	4.3	[7]
H_2	0.162	6.813	[8]
Ne	1.42	8.03	[9]
NaCl	23.83	5.09	[10]
Ar	4.13	5.77	[11]

References: [1] Occelli et al. (2003); [2] Hanfland et al. (2002); [3] Knittle (1995); [4] Dewaele et al. (2004); [5] Takemura (2007); [6] Speziale et al. (2001); [7] Syassen (2008); [8] Loubeyre et al. (1996); [9] Dewaele et al. (2008); [10] Dorogolupets and Dewaele (2007); [11] Jephcoat (1998).